SCIENCE CHINA
Technological Sciences

•Article•

January 2023 Vol.66 No.1: 204–214
https://doi.org/10.1007/s11431-022-2113-y

Calculating electron-phonon coupling matrix: Theory introduction, code development and preliminary application

YE YaoKun[1], WENG MouYi[1], ZHANG WenTao[1], LIN WeiCheng[1], CHEN TaoWen[1], PAN Feng[1*], ZHENG JiaXin[1*] & WANG Lin-Wang[2*]

[1] *School of Advanced Materials, Peking University, Shenzhen Graduate School, Shenzhen 518055, China;*
[2] *Institute of Semiconductors, Chinese Academy of Sciences, Beijing 100083, China*

Received April 25, 2022; accepted June 13, 2022; published online December 28, 2022

Electron-phonon coupling (EPC) in bulk materials is an important effect in multifarious physical and chemical phenomena. It is the key to explaining the mechanisms for superconductivity, electronic transport, etc. The EPC matrix describes the coupling of the electronic eigenstates of the studied system under the perturbation of phonons. Although the EPC matrix is closely relevant to many fundamental physicochemical properties, it remains a challenge to calculate the EPC matrix precisely due to the high computational cost. In recent years, Giustino et al. developed the EPW method on open-source *ab-initio* software Quantum Espresso, which uses Wannier functions (WFs) to calculate EPC matrix. However, due to the limitation of their implementation, it is not possible yet to calculate the EPC matrix under some important computational conditions, e.g., for DFT+U and HSE calculation. Given the importance of these computational conditions (e.g., for transition metal oxides), we have developed our own implementation of EPC matrix calculation based on the domestic *ab-initio* software PWmat. Our code allows the DFT+U and HSE correction, so we can get a more accurate EPC matrix in the related problems. In this article, we will first review the formulae and elucidate how to calculate the EPC matrix by constructing WFs. Then we will introduce our code along with its workflow on PWmat and present our test results of two classical semiconductor systems AlAs and Si, showing consistency with EPW. Next, the EPC matrix of $LiCoO_2$, a classical cathode material for lithium-ion batteries, is calculated using different exchange correlation (XC) functionals including LDA, PBE, DFT+U and HSE. A comparison is provided for the related EPC matrix. It shows there could be a significant difference for the EPC matrix elements due to the use of different XC functionals. Our implementation thus opens the way for fast calculation of EPC for the important class of materials, like the transition metal oxides.

electron-phonon coupling, Wannier functions, PWmat, Quantum Espresso, methods

Citation: Ye Y K, Weng M Y, Zhang W T, et al. Calculating electron-phonon coupling matrix: Theory introduction, code development and preliminary application. Sci China Tech Sci, 2023, 66: 204–214, https://doi.org/10.1007/s11431-022-2113-y

1 Introduction

A solid is a complex many-body macroscopic system composed of microscopic particles on the order of 10^{23}. The starting point of solid theory is to explain the various properties of solids and clarify the physical principles from a microscopic perspective. Phonons, as the quantum descriptor of lattice vibration, together with electrons are the basic research objects of solid theory, which determine many physical and chemical properties of solids such as band structure, lattice heat capacity and structural spectrum [1–3]. The movement of electrons in a solid lattice is affected by phonon scattering, and this type of electron-phonon interaction is defined as electron phonon coupling (EPC). Numerous physicochemical properties of solid materials are

*Corresponding authors (email: panfeng@pkusz.edu.cn; zhengjx@pkusz.edu.cn; lwwang@semi.ac.cn)

connected with EPC, such as superconductivity and carrier transport [4,5]. These important physical and chemical phenomena can be better explained and understood from the perspective of microscopic mechanisms through the in-depth study of EPC. Therefore, the study of EPC has universal significance and has attracted extensive attention for a long time. EPC has flourished in the experimental fields especially in recent years. For example, there is experimental evidence that the performance of carbon-based field-effect devices may be affected by phonon-limited carrier lifetime [6].

The physical concept of EPC can be traced back to 1929, when Bloch mentioned "*The interaction of the electrons and the elastic waves of the lattice*" [7] to discuss the Schrödinger equation in periodic potentials. Soon after several years, "lattice elastic wave" was replaced by the concept of "phonon". Despite the long history of EPC study, the development of EPC in theoretical calculation has not been a smooth path since the direct calculation of EPC requires a large amount of computation. The primary target of the theoretical calculation of EPC is to obtain the so-called EPC matrix, which is a core parameter to describe the physicochemical phenomena related to EPC. EPC matrix g can be written as

$$g(m\mathbf{k}_1, n\mathbf{k}_2, b\mathbf{q}) = \left\langle \psi_{m\mathbf{k}_1} \left| \frac{\partial H}{\partial v_{b\mathbf{q}}} \right| \psi_{n\mathbf{k}_2} \right\rangle. \quad (1)$$

In eq. (1), $\psi_{m\mathbf{k}_1}$ is the wavefunction with electron band index m and crystal momentum $\mathbf{k}_1$ in Brillouin zone, $\psi_{n\mathbf{k}_2}$ is the wavefunction with electron band index n and crystal momentum $\mathbf{k}_2$ in Brillouin zone, H is the Hamiltonian of the studied system and $\boldsymbol{v}_{b\mathbf{q}}$ indicates the normal coordinates under the phonon mode with phonon band index b and crystal momentum $\mathbf{q}$ in Brillouin zone. EPC matrix describes the interaction between $\psi_{m\mathbf{k}1}$ and $\psi_{n\mathbf{k}_2}$ under the specific phonon modes scattering.

Despite the significant importance of EPC, the research on EPC has been a technical bottleneck for a long time. The main technical difficulty is the large consumption of computing resources brought by EPC matrix. In order to solve the technical barriers, the basic theoretical research of EPC has also undergone many explorations historically. As early as 1950, Bardeen and Shockley [8] proposed deformation potential approximation (DPA) and gained wide acceptance. DPA assumed that phonon energy is much smaller than electron energy at the long-wavelength acoustic phonon modes, and electron energies in both initial and final states remain equal. Thus, electrons are affected by elastic scattering and EPC can be approximately linearly related to the phonon wave vector $\mathbf{q}$, which simplifies the calculation of the EPC matrix. Although DPA has achieved success in some systems, the theoretical model is ultimately too simplified to be widely and universally applied, and does not fundamentally solve the real technical difficulties of EPC. In 2007, Giustino et al. [9] proposed that Wannier functions (WFs) can be used to quickly and accurately calculate the EPC matrix. The theoretical foundation is that the WFs in real space and Bloch functions in reciprocal space are in Fourier transform relationships with each other. This transformation process can theoretically guarantee the calculation accuracy. However, only a few DFT calculations are required by utilizing the highly localized property of WFs, which can quickly obtain the corresponding EPC matrix information. After nearly ten years of development and improvement, Giustino et al. [9–11] integrated the code of this method into the EPW package in the open-source software Quantum Espresso. Besides, some pioneering efforts by PERTURBO group [12–14] and ABINIT group [15,16] have also facilitated the flourishing of EPC research field.

In this paper, given the importance of EPC and according to the theoretical method mentioned above, we developed this code on the domestic software PWmat [17,18] as shown in Figure 1. We have obtained the results basically consistent with EPW in the test systems, realizing the autonomy of this module. Next, we briefly describe the theory and the workflow in PWmat, and present computational results of two classical semiconductor systems, AlAs and Si. In addition, we also introduced DFT+U and HSE corrections in the code workflow to expand the research objects to some systems with strong correlation interactions. We will discuss the influence of different functionals on the EPC matrix using $LiCoO_2$, a classic Li-ion battery cathode material. Moreover, our code also implements more independent degrees of freedom for users, and information about the range of indicators of interest can be obtained through a simple input file.

2 Related theory and code process

2.1 Lattice dynamics

Lattice vibrations are considered as one of the most im-

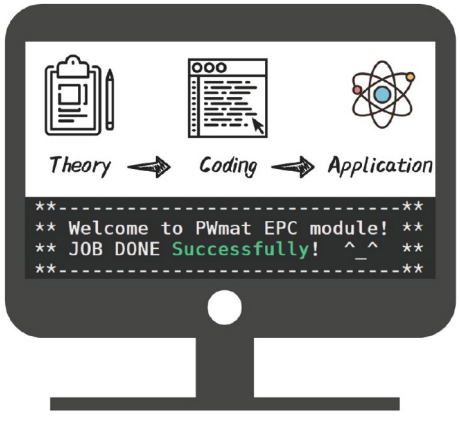

Figure 1 (Color online) Electron phonon coupling matrix now can be calculated using self-developed code on domestic software PWmat.

portant and successful chapters in modern solid theory [19,20]. Through the theory of lattice vibrations, people have established the physical concept of "phonon", a theoretical image to describe the collective vibrations. Phonons have been widely used to study the spectral properties such as infrared spectroscopy and Raman spectroscopy and thermodynamic properties such as specific heat capacity and heat conduction [1–3]. The concept of phonon is also an important component in the theory of EPC. Therefore, a brief introduction to lattice vibrations will help us better understand the theoretical image of EPC, and it will be further used for the derivation of subsequent EPC related formulae.

We consider a unit cell containing M atoms and indicate each atom with an index κ, κ=1,2,3,…,M. Their Cartesian coordinates are denoted as $\tau_{\kappa\alpha}$, where α indicates x, y, z directions. Born-von Kármán boundary conditions are used to describe the periodic properties of solids. We then consider a supercell containing N_{p} unit cells and indicate each unit cell with an index $\mathbf{R}_{\mathrm{p}}$, $\mathbf{R}_{\mathrm{p}}$=1,…,N_{p}. Thus, the Cartesian coordinates of an atom κ of unit cell p in its equilibrium position can be denoted as $\tau^{0}_{\kappa\alpha\mathbf{R}_{\mathrm{p}}}$ and the atomic displacement from its equilibrium position can be denoted as $\tau_{\kappa\alpha\mathbf{R}\mathrm{p}}$.

First we need to introduce harmonic approximation in order to describe lattice dynamics, according to which the total potential energy U can be expanded to second-order in the atomic displacement $\tau_{\kappa\alpha\mathbf{R}\mathrm{p}}$ (orders higher than second-order are omitted in harmonic approximation):

$$U = U_0 + \frac{1}{2}\sum_{\kappa\alpha\mathbf{R}_{\mathrm{p}}\kappa'\alpha'\mathbf{R}'_{\mathrm{p}}} \frac{\partial^2 U}{\partial\tau_{\kappa\alpha\mathbf{R}_{\mathrm{p}}}\partial\tau_{\kappa'\alpha'\mathbf{R}'_{\mathrm{p}}}}\tau_{\kappa\alpha\mathbf{R}_{\mathrm{p}}}\tau_{\kappa'\alpha'\mathbf{R}'_{\mathrm{p}}}. \tag{2}$$

In eq. (2), U_0 is the total potential energy when the atoms are in their equilibrium positions, and we can define the second derivatives of total potential energy U as "interatomic force constants":

$$C_{\kappa\alpha\mathbf{R}_{\mathrm{p}}\kappa'\alpha'\mathbf{R}'_{\mathrm{p}}} = \frac{\partial^2 U}{\partial\tau_{\kappa\alpha\mathbf{R}_{\mathrm{p}}}\partial\tau_{\kappa'\alpha'\mathbf{R}'_{\mathrm{p}}}}. \tag{3}$$

Eq. (3) denotes the force on atom κ of unit cell p along α direction when the atom κ' of unit cell p' is displaced along α' direction, and thus it is called "interatomic force constants".

The Fourier transform of eq. (3) leads to the "dynamical matrix":

$$D_{\kappa\alpha,\kappa'\alpha'}(\mathbf{q}) = \frac{1}{\sqrt{M_\kappa M_{\kappa'}}}\sum_{\mathbf{R}_{\mathrm{p}}} C_{\kappa\alpha 0,\kappa'\alpha'\mathbf{R}_{\mathrm{p}}} \mathrm{e}^{\mathrm{i}\mathbf{q}\cdot\mathbf{R}_{\mathrm{p}}}. \tag{4}$$

In eq. (4), M_κ is the mass of atom κ and $\mathbf{q}$ is the crystal momentum for phonon in Brillouin zone. The eigen equation of dynamical matrix is

$$\sum_{\kappa'\alpha'} D_{\kappa\alpha,\kappa'\alpha'}(\mathbf{q})\xi_{\kappa'\alpha',b\mathbf{q}} = \omega^2_{\mathbf{q}b}\xi_{\kappa\alpha,b\mathbf{q}}. \tag{5}$$

In eq. (5), $\omega_{\mathbf{q}b}$ is the vibration frequency with phonon branch index b (b = 1, 2, 3,...,3M) and phonon crystal momentum $\mathbf{q}$ in Brillouin zone. $\xi_{\kappa\alpha,b\mathbf{q}}$ is the "normal modes of vibration" or "polarization of the vibration wave" [4,9], which describes the atomic vibration modes for each unit cell at given phonon branch b and phonon crystal momentum $\mathbf{q}$. $\xi_{\kappa\alpha,b\mathbf{q}}$ contains the "information of collective motion of atoms" [20] and can be normalized and orthogonalized as follows:

$$\sum_{\kappa\alpha}\xi^{*}_{\kappa\alpha,b\mathbf{q}}\xi_{\kappa\alpha,b'\mathbf{q}} = \delta_{bb'}, \tag{6}$$

$$\sum_{b}\xi^{*}_{\kappa'\alpha',b\mathbf{q}}\xi_{\kappa\alpha,b\mathbf{q}} = \delta_{\kappa\kappa'}\delta_{\alpha\alpha'}. \tag{7}$$

Utilizing the orthogonality and completeness properties of normal modes, lattice vibrations can be represented as a linear combination [19]:

$$\tau_{\kappa\alpha\mathbf{R}_{\mathrm{p}}} = \frac{1}{\sqrt{M_\kappa}}\sum_{\mathbf{q},b}\xi_{\kappa\alpha,b\mathbf{q}}v_{b\mathbf{q}}\mathrm{e}^{\mathrm{i}\mathbf{q}\cdot\mathbf{R}_{\mathrm{p}}}. \tag{8}$$

In eq. (8), $v_{b\mathbf{q}}$ is the normal coordinates with phonon branch b and phonon crystal momentum $\mathbf{q}$. Therefore, there are two main primary tasks in the actual phonon-related calculations using *ab-initio* software: (1) to obtain the relevant information of the phonon vibration frequency, namely the $\omega_{\mathbf{q}b}$-q dispersion relation (phonon spectrum); (2) to obtain the relevant information on the phonon vibration modes, namely $\xi_{\kappa\alpha,b\mathbf{q}}$.

2.2 Wannier functions (WFs)

Ideal crystals are characterized by strict periodicity. Bloch's theorem indicates that the wavefunction of a single-electron in periodic potentials is an amplitude-modulated plane-wave, which can be written as

$$|\psi_{n\mathbf{k}}(\mathbf{r})\rangle = \mathrm{e}^{\mathrm{i}\mathbf{k}\cdot\mathbf{r}}|u_{n\mathbf{k}}(\mathbf{r})\rangle. \tag{9}$$

In eq. (9), n is the electron band index, $\mathbf{k}$ is the crystal momentum in Brillouin zone and $u_{n\mathbf{k}}(\mathbf{r})$ is a periodic function of real space. $\psi_{n\mathbf{k}}(\mathbf{r})$ is also called "Bloch functions" (BFs). For current first-principles density functional theory calculations, the use of the BFs to describe the electronic structures of a solid system is widespread, which is called the Bloch representation. Through the representation transformation, we can change from Bloch representation to Wannier representation and use the WFs to describe the electronic structure information of the studied system [21,22]. The conversion relationship between BFs and WFs is

$$|W_m(\mathbf{r}+\mathbf{R})\rangle = \frac{1}{N}\sum_{n\mathbf{k}}\mathrm{e}^{\mathrm{i}\mathbf{k}\cdot\mathbf{R}}U_{nm,\mathbf{k}}|\psi_{n\mathbf{k}}(\mathbf{r})\rangle, \tag{10}$$

or

$$|\psi_{n\mathbf{k}}(\mathbf{r})\rangle = \sum_{m\mathbf{R}}\mathrm{e}^{-\mathrm{i}\mathbf{k}\cdot\mathbf{R}}U^{\dagger}_{mn,\mathbf{k}}|W_m(\mathbf{r}+\mathbf{R})\rangle. \tag{11}$$

In eqs. (10) and (11), N is the number of unit cells in the supercell that we used to construct WFs, $W_m(\mathbf{r}+\mathbf{R})$ denotes the Wannier function localized in unit cell $\mathbf{R}$ with band index

m and $U_{nm,\mathbf{k}}$ is the unitary transformation matrix between BFs and WFs. Usually WFs are highly localized as shown in Figure 2, thus WFs are often chosen as the basis set for the tight-binding model [23,24], which can be normalized as follows:

$$\left\langle W_m(\mathbf{r}+\mathbf{R})\middle|W_n(\mathbf{r}+\mathbf{R}')\right\rangle = \delta_{mn}\delta_{\mathbf{R}\mathbf{R}'}. \tag{12}$$

The phase arbitrariness of BFs may lead to the arbitrariness of the selection of the unitary transformation matrix, which is also called the "gauge freedom" of WFs [22]. Now a general and widely used approach is the "maximally localized Wannier functions" method proposed by Marzari and Vanderbilt [23].

Based on eqs. (8) and (11), we can expand the EPC matrix using WFs:

$$g(m\mathbf{k}_1, n\mathbf{k}_2, b\mathbf{q}) = \sum_{\mathbf{R}'_e,\mathbf{R}_e} e^{ik_1\mathbf{R}'_e}e^{-ik_2\mathbf{R}_e} \times \sum_{m',n',\kappa\alpha} \frac{\xi_{\kappa\alpha,b\mathbf{q}}}{\sqrt{M(\kappa)}} U_{mm',\mathbf{k}_1} g\left(m'\mathbf{R}'_e, n'\mathbf{R}_e, \kappa\alpha\mathbf{R}_p\right) U^{\dagger}_{n'n,\mathbf{k}_2}. \tag{13}$$

In eq. (13), $g\left(m'\mathbf{R}'_e, n'\mathbf{R}_e, \kappa\alpha\mathbf{R}_p\right)$ can be written as

$$g\left(m'\mathbf{R}'_e, n'\mathbf{R}_e, \kappa\alpha\mathbf{R}_p\right) = \left\langle W_{m'}(\mathbf{r}+\mathbf{R}'_e)\middle|\frac{\partial H}{\partial\tau_{\kappa\alpha\mathbf{R}_p}}\middle| W_{n'}(\mathbf{r}+\mathbf{R}_e)\right\rangle. \tag{14}$$

Thus, we can calculate the EPC matrix under the Wannier representation in order to utilize the highly localized property of WFs. The specific process is shown in Figure 3. Figure 3(a) is a schematic diagram of an ideal crystal without considering lattice vibrations, and Figure 3(b) is a schematic diagram of calculating the EPC matrix using WFs under Wannier representation. When we perturb atom κ in unit cell $\mathbf{R}_p$ and the unit cell index of WFs are denoted as $\mathbf{R}_e$, $\mathbf{R}'_e$, due to the advantages of highly localized WFs, "*whenever two of these functions are centered on distant unit cells, the e-ph matrix element in the Wannier representation vanishes*" [9]. Therefore, we only need to calculate eq. (14) using WFs, and then we can obtain the EPC matrix information according to eq. (13).

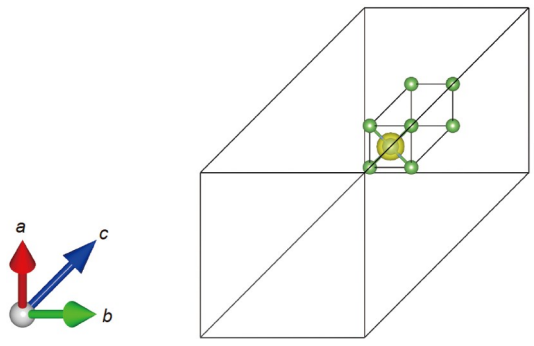

Figure 2 (Color online) Schematic diagram of localized WFs.

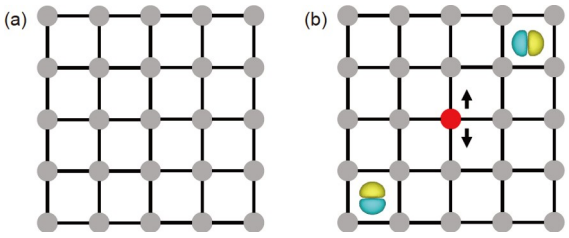

Figure 3 (Color online) (a) Schematic diagram of ideal crystal; (b) schematic diagram of EPC in Wannier representation

2.3 Code workflow

Below, we briefly describe our code workflow for specific computing operations. Based on the relevant formulae mentioned above, we need to do the following things shown in Figure 4 first if we want to get EPC matrix.

(a) Prepare PWmat input files and perform DFT calculations to obtain electron-related information (electron information) and phonon-related information (phonon information);

(b) Construct WFs;

(c) Calculate eq. (14) using WFs and convert it back to eq. (1), namely EPC calculations;

(d) Get EPC output files.

2.4 Computational details

In this work, we show our calculation results and their comparison with EPW on two classical semiconductor systems, AlAs and Si. Then we introduce the correction of DFT +U (U value 3.4 eV [25]) and HSE [26] in the $LiCoO_2$ system and show the corrected EPC matrix. The self-consistent calculation of the electronic structure is completed using the domestic plane wave first-principles software PWmat [17,18], and the k-point grid sampling is 4 × 4 × 4 for the

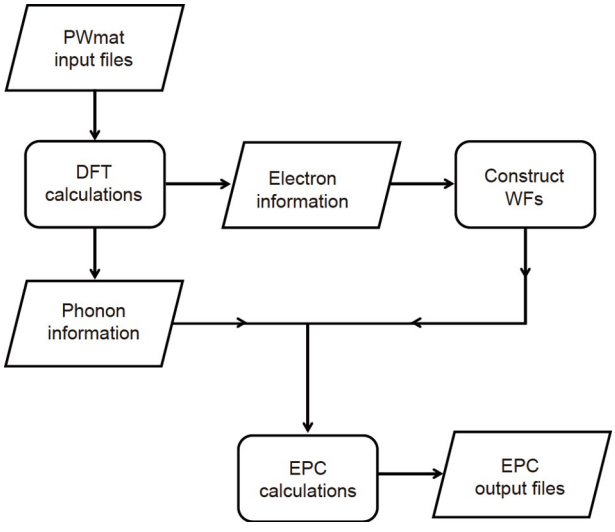

Figure 4 The whole workflow of our code.

following constructions of WFs and the calculation of EPC matrix. WFs are constructed using Wannier90 code [27]. Phonon-related information is calculated using supercell method of Phonopy [20] in an interface with PWmat. The EPC matrix calculation is done using supercell method to generate the change of Hamiltonian due to phonons based on our self-developed code. Crystal structures are taken from MaterialGo database (http://www.pkusam.com/) contributed by School of Advanced Materials, Peking University [28].

3 Results and discussion

3.1 Comparison of calculation results of AlAs system and Si system with EPW

III–V compound semiconductors provide the material basis for some mature commercial technologies and cutting-edge electronic devices, which have important applications in the fields of light-emitting diodes and photodetectors [29]. AlAs is a typical representative of III–V compound semiconductors. Meanwhile, Si is a semiconductor material widely used in information science, material science, aerospace and other fields [30,31]. Figures 5(a)–(c) and 6(a)–(c) show the WFs plots, electronic structures and phonon structures of AlAs and Si, respectively. We selected all the valence bands of AlAs to construct WFs, corresponding to the 1s and 3p orbitals of Al atom and 1s and 3p orbitals of As atom (energy bands in Figure 5(b)). For the WFs construction of Si, we selected four valence bands and four conduction bands and there existed sp3 hybridization among these orbitals (energy bands in Figure 6(b)). As for the phonon information, the main phonon modes of AlAs and Si are two degenerate transverse acoustic modes, one longitudinal acoustic mode, and two degenerate transverse optical modes and one longitudinal optical mode. The corresponding degeneracy can also be seen in the EPC matrix shown later. Tables 1 and 2 demonstrate the EPC matrix values calculated by our code and EPW code, respectively. The EPC matrix values are shown in the form of the square moduli in units of meV proposed by Poncé et al. [10,32]. The AlAs system in Table 1 shows the EPC matrix values between 4 groups of different **k** points on the set of non-degenerate energy bands of eq. (1) with band index $m = n = 5$; the Si system in Table 2 shows the EPC matrix values between 4 groups of different **k** points on the sp3 hybrid energy bands of eq. (1) with band index $m = n = 8$. Both AlAs and Si were calculated using PBE functional. Under the premise of using the same calculation parameters, the calculation results of our code are basically the same as EPW, which indicates our code achieves preliminary success.

There are nevertheless some differences. In some EPC matrix elements, EPW results are exact zero, but our results have small values (like 0.035 meV). We believe this is because EPW has enforced the symmetry operation, while our implementation has not. Therefore the small values like 0.035 meV are probably due to some numerical errors. Nevertheless, we believe such a small error should not cause any practical problems. In reality, some finite temperature effects or anharmonic effects might induce much larger coupling than these numerical errors. There are also other cases, where EPW results are not zero but rather small (like 0.0006 meV) while our results are much larger (like

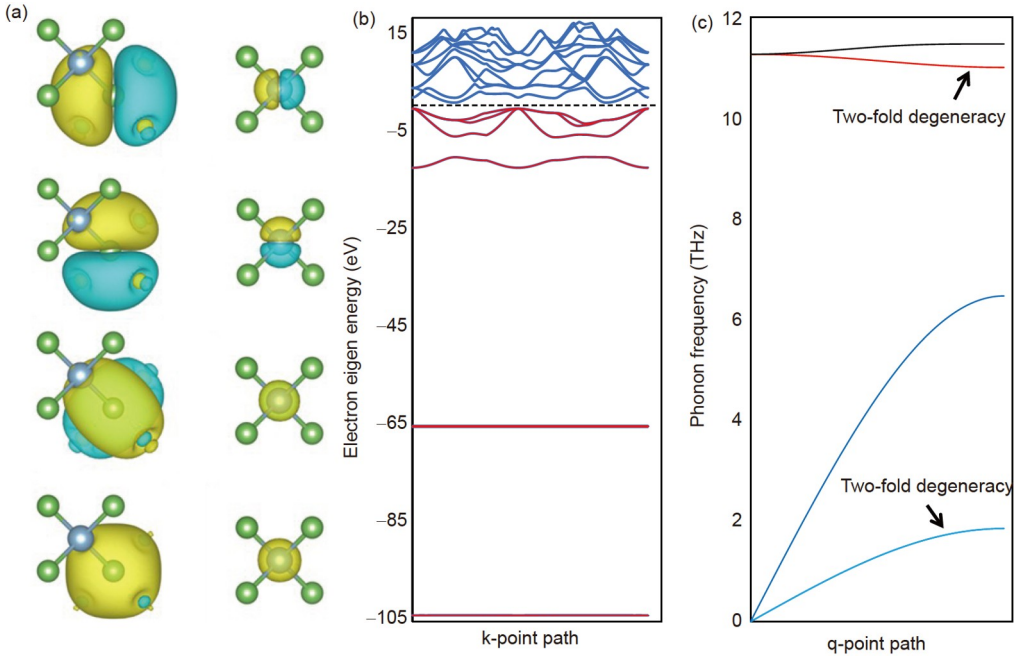

Figure 5 (Color online) (a) WFs plots; (b) electronic structure; (c) phonon structure of AlAs.

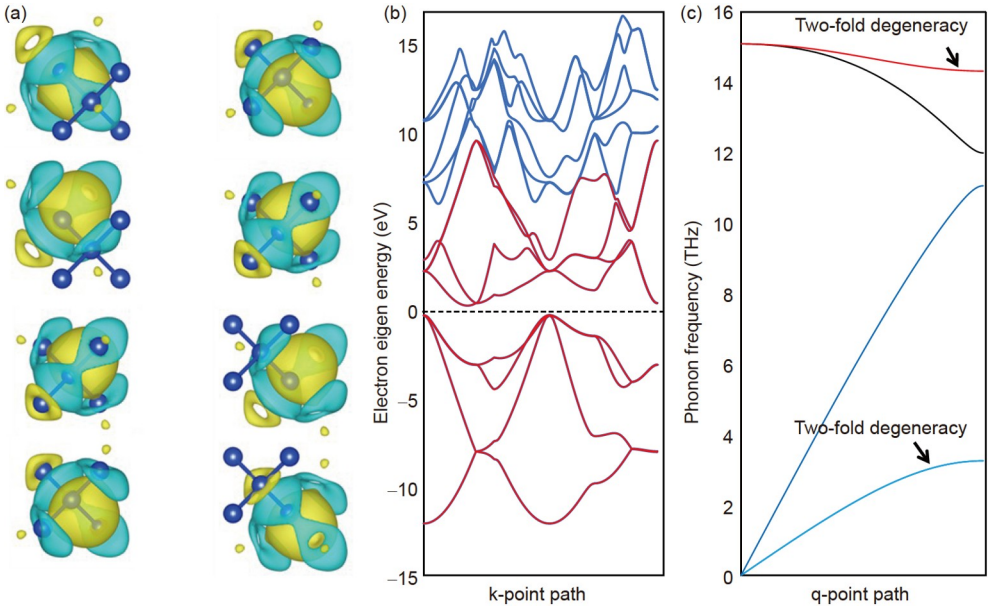

Figure 6 (Color online) (a) WFs plots; (b) electronic structure; (c) phonon structure of Si.

Table 1 The EPC matrix of AlAs

	Phonon branch index	EPW results (meV)	PWmat results (meV)
$\mathbf{k}_1$=(0,0,0) $\mathbf{q}$=(0,0,0.25) $\mathbf{k}_2$=(0,0,0.25)	1	0.0000	0.0578
	2	0.0000	0.0578
	3	102.9653	104.9915
	4	0.0000	0.0394
	5	0.0000	0.0394
	6	156.8399	151.6571
$\mathbf{k}_1$=(0,0,0) $\mathbf{q}$=(0,0,0.5) $\mathbf{k}_2$=(0,0,0.5)	1	0.0000	0.0350
	2	0.0000	0.0350
	3	69.2065	66.1230
	4	0.0000	0.0096
	5	0.0000	0.0096
	6	170.7382	174.7588
$\mathbf{k}_1$=(0,0,0.25) $\mathbf{q}$=(0,0,0.25) $\mathbf{k}_2$=(0,0,0.5)	1	0.0000	0.0701
	2	0.0000	0.0701
	3	50.5914	50.6360
	4	0.0000	0.0443
	5	0.0000	0.0443
	6	183.4980	180.3063
$\mathbf{k}_1$=(0,0,0.5) $\mathbf{q}$=(0,0.25,0.25) $\mathbf{k}_2$=(0,0.25,0.75)	1	20.9429	18.7558
	2	20.9429	18.7558
	3	57.7475	56.7075
	4	21.1091	19.9562
	5	21.1091	19.9562
	6	151.1388	153.7232

Table 2 The EPC matrix of Si

	Phonon branch index	EPW results (meV)	PWmat results (meV)
$\mathbf{k}_1$=(0,0,0) $\mathbf{q}$=(0,0,0.25) $\mathbf{k}_2$=(0,0,0.25)	1	0.0050	2.0173
	2	0.0050	2.0173
	3	90.0553	97.8114
	4	27.3687	26.1559
	5	0.0047	1.0738
	6	0.0047	1.0738
$\mathbf{k}_1$=(0,0,0) $\mathbf{q}$=(0,0.25,0.25) $\mathbf{k}_2$=(0,0.25,0.25)	1	110.6513	123.2564
	2	110.6513	123.2564
	3	0.0008	1.9838
	4	9.8373	10.1946
	5	9.8373	10.1946
	6	0.0020	2.1024
$\mathbf{k}_1$=(0,0,0.25) $\mathbf{q}$=(0,0.25,0.25) $\mathbf{k}_2$=(0,0.25,0.5)	1	78.3118	85.5786
	2	78.3118	85.5786
	3	0.0006	1.7073
	4	13.4337	13.4007
	5	13.4337	13.4007
	6	0.0007	1.5527
$\mathbf{k}_1$=(0,0,0.5) $\mathbf{q}$=(0,0.25,0) $\mathbf{k}_2$=(0,0.25,0.5)	1	186.6554	195.9615
	2	186.6554	195.9615
	3	0.0017	1.7022
	4	0.0008	0.7844
	5	33.1877	30.6855
	6	33.1877	30.6855

1.7 meV). We feel such elements should also be zero, and the EPW symmetry enforcement is not complete. Therefore, for this symmetry case, our numerical error (without symmetry enforcement) can be around 2 meV. Compared with other truly nonzero coupling constants, this error is at least one order of magnitude smaller, or could be two orders of magnitude smaller.

3.2 Comparison and discussion of different functionals in $LiCoO_2$ system

$LiCoO_2$ is a classic layered cathode material for lithium-ion batteries with high theoretical capacity and good electrical conductivity, and has been successfully commercialized on a large scale [33–36]. $LiCoO_2$ has a significantly strong correlation effect since Co is a typical transition metal. Usually, it is necessary to introduce DFT+U or HSE to modify its electronic structure in theoretical calculations. Therefore, a natural question is: since the electronic structure needs to be corrected using higher-order functionals, how much EPC matrix will be affected by different functionals? According to the current research basis and frontier progress, the effect of different functionals on the values of EPC matrix is unknown. Based on this problem, we calculated and compared the EPC matrix of $LiCoO_2$ system at its valence band maximum (VBM) with band index $m = n = 16$, $\mathbf{k}_1 = (0,0,0)$ and $\mathbf{q} = (0,0,0.25)$ under several different functional choices of LDA, PBE, LDA+U, PBE+U and HSE. Since EPC matrix is directly affected by the computational accuracy of the electronic structure part and the phonon structure part, we systematically compared the effects of different functionals for both parts. The plots of electronic band structures and phonon spectrums of $LiCoO_2$ are shown in Supporting Information, Figure S1. In the following discussion, "LDA-PBE results" means that the electronic structure is calculated using LDA and the phonon structure is calculated using PBE, and so on for the rest.

Since there is no direct experimental data to compare with EPC matrix, a natural question is how do we judge the accuracy of the EPC matrix under different functionals from the perspective of pure theoretical calculation? Zhou et al. [13] reported that the phonon spectrum of CoO system demonstrated imaginary frequencies when the calculation of phonon structure part did not take DFT+U into account. In contrast, the imaginary frequencies were eliminated after implementing DFT+U, so they suggest that studies on EPC effect in correlated systems should introduce DFT+U correction. This is obviously consistent with people's expected cognition. When we use higher-precision calculation methods to calculate the electronic structure and phonon structure, we should get more accurate EPC matrix values. Our calculation results show that there are still differences in the values of EPC matrix under different functionals, and the values of EPC matrix should be jointly affected by both electronic structure part and phonon structure part. Therefore, we think that the influence of these two parts on the values of EPC matrix under different functionals should be discussed separately to help us better understand the differences of EPC matrix values under different functionals.

First, we keep the functionals selected for electronic structure and phonon structure consistent and we define this situation as Case 1, then check and analyze the changes of EPC matrix values as shown in Figure 7. In Figure 7, the horizontal axis is phonon branch index, and the vertical axis is the value of EPC matrix (in the unit of meV). Figure 7 shows that when electronic structure and phonon structure adopt the same functional, the "EPC matrix value-phonon branch" images drawn under different functionals show some consistent behaviors. In the acoustic branches (corresponding to phonon branch indexes 1–3), the EPC matrix values are relatively small, and the EPC matrix values at the seventh and the tenth branches are close to zero, indicating that under these phonon modes, the electron eigenstates are weakly affected by phonon scattering. The maximum values of the EPC matrix are obtained at the eleventh branch for all the different functionals. However, there are still some different behaviors among different functionals. For LDA-LDA, the maximum value of the EPC matrix is relatively small compared with the maximum value of other functionals, and the values in the fourth branch and the ninth branch are obviously smaller than other functionals. In addition, the EPC matrix value of the ninth branch is significantly smaller than that of the eighth branch. The relative trend of these two branches in LDA-LDA is opposite to that of LDAU-LDAU, PBEU-PBEU, and HSE-HSE. PBE-PBE shows a similar behavior to LDA-LDA, but its maximum value is larger than that of LDA-LDA, and the EPC matrix

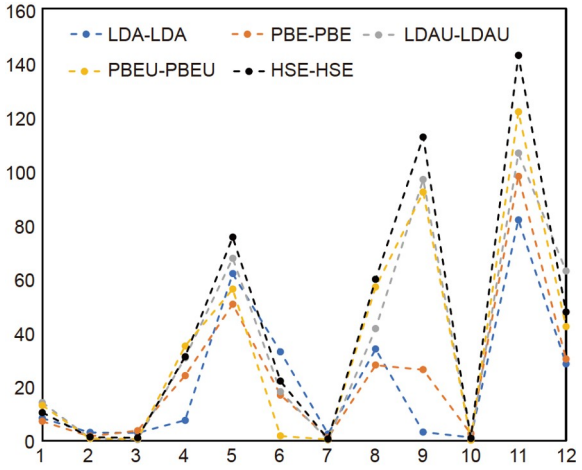

Figure 7 (Color online) The comparison of EPC matrix of $LiCoO_2$ using different functionals for electronic structures and phonon structures. Horizontal axis: phonon branch index; vertical axis: the value of EPC matrix (meV).

value of the ninth branch is just slightly lower than that of the eighth branch. The EPC matrix values of LDAU-LDAU are larger than those of LDA-LDA and PBE-PBE in general. PBEU-PBEU is similar to LDAU-LDAU, but its EPC matrix value suddenly drops to almost zero at the sixth branch. The behavior of HSE-HSE is close to that of PBEU-PBEU, and its amplitude is larger than that of PBEU-PBEU. Then, what caused these differences and similar behaviors of the EPC matrix values under different functionals? What are the roles of electronic structure part and phonon structure part under different functionals? Therefore, we further discuss the effects of the electronic structure part and phonon structure part on the EPC matrix separately.

We first discuss the case that we fix the functional selection of the electronic structure part and use PBE for all situations, to explore the influence of different functionals of phonon structure part on the values of the EPC matrix, as shown in Figure 8, which is defined as Case 2. We still look at the overall picture first. Figure 8 shows that when the electronic structure is fixed using PBE functional, the "EPC matrix value-phonon branch" image plotted under different functionals still shows some consistent behaviors. The EPC matrix values in the acoustic modes are relatively small, the EPC matrix values at the seventh and the tenth branches are all close to zero, and the EPC matrix will obtain the maximum value at the eleventh branch for all the different functionals, which is almost consistent with the trend in Figure 7. In addition, the different behaviors among different functionals in Figure 8 are also very similar to the trend in Figure 7. For PBE-LDA, it is still obviously smaller at the fourth and ninth branches. Meanwhile, the value of the ninth branch is still significantly reduced compared with the eighth value, and the relative trend of these two branches is still opposite to that of PBE-LDAU, PBE-PBEU, and PBE-HSE. Besides, PBE-PBEU still suddenly drops to zero at the sixth branch. But the difference between Case 1 and Case 2 is that when the electron functional is fixed in PBE, the amplitude of the EPC matrix is regulated. For example, the amplitude of PBE-HSE is significantly lower than that of HSE-HSE. Besides, the amplitude of PBE-LDAU and that of PBE-HSE are basically the same. In short, when the electronic structure functional is fixed using PBE and phonon structure functional changes, the overall behavior of the EPC matrix values at different phonon branches in Case 2 remains almost consistent with Case 1, and the only difference is the amplitude of the EPC matrix values. The comparison between Case 1 and Case 2 leads us to conjecture that the influence of the electronic structure on the values of the EPC matrix is mainly reflected in its amplitude, and the performance of the EPC matrix values at different phonon branches is mainly affected by the functional selection of the phonon structure.

Therefore, we discuss the case that we fix the functional selection of phonon structure part and use PBE for all situations to investigate the influence of different functionals in the electronic structure part on the values of the EPC matrix, as shown in Figure 9, which is defined as Case 3. We still analyze the overall picture first. Figure 9 shows that when the phonon structure is fixed using PBE functional, the "EPC matrix value-phonon branch" image under different functionals at different phonon branches demonstrate almost the same behaviour. The values of the EPC matrix in acoustic modes are relatively small, the values of the EPC matrix at the seventh branch and the tenth branch are close to zero, and maximum values are obtained at the eleventh branch for all the different functionals. In addition, the EPC matrix values of the ninth branch of different functionals show a downward trend compared with the eighth branch, especially for LDAU-PBE, PBEU-PBE, and HSE-PBE. This behavior is opposite to that of LDAU-LDAU, PBEU-PBEU and HSE-

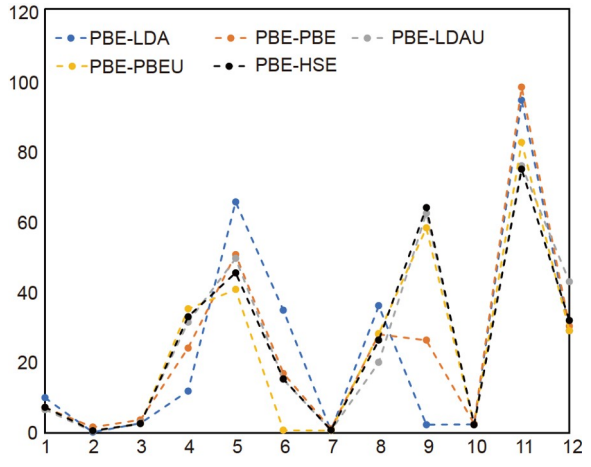

Figure 8 (Color online) The comparison of EPC matrix of $LiCoO_2$ using different functionals for phonon structures with PBE electronic structures. Horizontal axis: phonon branch index; vertical axis: the value of EPC matrix (meV).

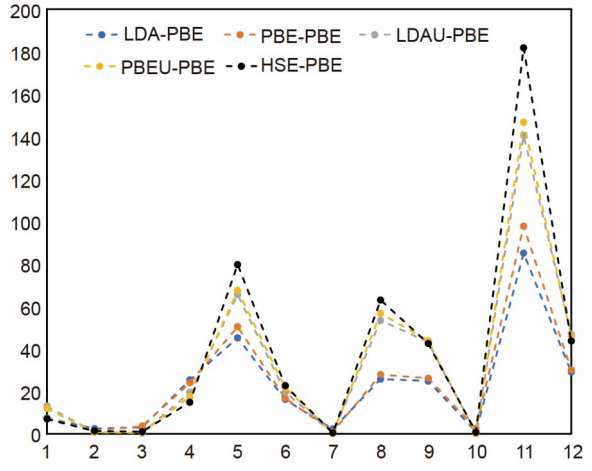

Figure 9 (Color online) The comparison of EPC matrix of $LiCoO_2$ using different functionals for electronic structures with PBE phonon structures. Horizontal axis: phonon branch index; vertical axis: the value of EPC matrix (meV).

HSE in Case 1. In short, when the phonon structure part is fixed, the EPC matrix values behave almost the same on different phonon branches, but their amplitudes are tuned due to the different choices in the electronic structure. The results in Case 3 also support our conjecture proposed in Case 2.

Moreover, based on the above discussion and understanding, we laterally compare the electronic structure and phonon structure in Figure 10 under the selection of LDA and PBE, namely the values of EPC matrix for LDA-LDA, LDA-PBE, PBE-LDA, and PBE-PBE, respectively. When the functional selection changes from "LDA-LDA" to "PBE-LDA", the phonon structures are consistent, and the EPC matrix values are only regulated by the selection of the electronic structure functionals. Hence, the LDA-LDA and PBE-LDA lines in Figure 10 roughly overlap with only a numerical difference obtained by the correction of the electronic structure. When the functional selection changes from "LDA-LDA" to "LDA-PBE", the electronic structures are consistent, and the behavior of the EPC matrix values change at different phonon branches, so the LDA-LDA and LDA-PBE lines in Figure 10 demonstrate different behaviors. For example, the LDA-LDA and LDA-PBE lines give opposite results for phonon branches 4 and 5, as well as phonon branches 8 and 9. Therefore, when the functional selection changes from "LDA-LDA" to "PBE-PBE", the electronic structure part and the phonon structure part change simultaneously. Therefore, the EPC matrix will get a relatively large difference in calculation results. For other functionals, when the electronic structure and the phonon structure change simultaneously, the EPC matrix values will demonstrate different behaviors as shown in Figure 7. By analyzing the effects of the electronic structure part and phonon structure part respectively, we can see the "evolution" process of the EPC matrix under different functionals, which helps us better understand the calculation difference of the EPC matrix values under different functionals.

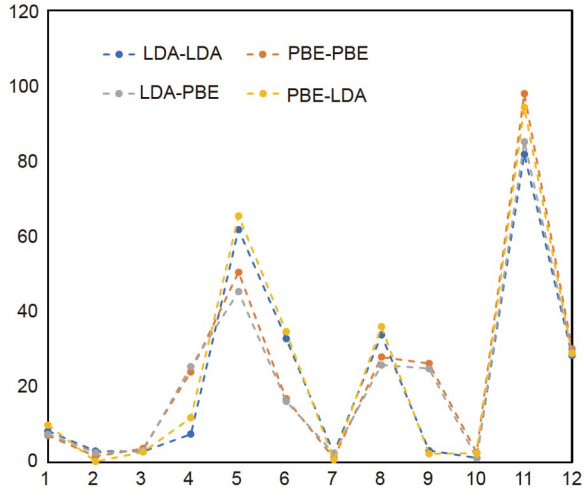

Figure 10 (Color online) The comparison of EPC matrix of $LiCoO_2$ using LDA and PBE for electronic structures and phonon structures. Horizontal axis: phonon branch index; vertical axis: the value of EPC matrix (meV).

Based on the above discussion, different functionals will lead to different EPC matrix results when choosing different electronic structures or different phonon structures. Specifically, the electronic structure part affects the relative amplitude of EPC matrix values at the same phonon branch, while the phonon structure part directly determines the relative amplitude of EPC matrix values between different phonon branches. The common influence of both parts may cause the values of EPC matrix to appear to be quite different, which indicates that more accurate functionals should be used in the calculation of EPC matrix whether in the electronic structure part or in the phonon structure part. In addition, although the EPC matrix values cannot be directly compared with the experimental values, the electronic structure and phonon structure can be compared with the experiments respectively as a side reference for the calculation of the EPC matrix. We choose the experimental band gap values as the reference index for the accuracy of the electronic structure part, and the peak positions of Raman spectrum in the experiment as the reference index for the accuracy of the phonon structure part. The calculation results and the experimental results of band gap values and Raman peak values under different functionals are shown in Table 3 [37–40] for comparison. Based on Table 3, we believe that for the calculation of the $LiCoO_2$ EPC matrix, the electronic structure part should at least reach the accuracy of PBE+U, and the phonon structure part should at least reach the calculation accuracy of PBE. Relatively speaking, for the calculation of EPC matrix, the PBE+U is close to HSE06 results for Case 1, Case 2, and Case 3. On the other hand, PBE is close to LDA results.

4 Conclusions

EPC affects many physicochemical properties of materials and is also the underlying mechanism of many important physicochemical phenomena. EPC matrix is a core parameter to describe the physicochemical phenomena related to EPC. However, the theoretical calculation of EPC matrix has been limited by its large consumption of computing resources for a long time, which significantly restricts the related studies of EPC. In recent years, Giustino et al. [9–11] developed the EPW method on Quantum Espresso. They proposed using Wannier functions to calculate the EPC matrix, making it possible to calculate the EPC matrix much more easily. In this paper, we first briefly introduce this theory. Based on this theory, we implement this module on the domestic software PWmat, and get the calculation results

Table 3 The comparison of properties of electronic and phonon structures of $LiCoO_2$ using different functionals

System	Gap (eV)	E_g mode Raman shift (cm^{-1})	A_{1g} mode Raman shift (cm^{-1})
Experiment	2.70 [37]	486 [38]	596 [38]
LDA	0.77	469.52	536.96
PBE	0.91	500.68	551.68
LDA+U	1.91	512.17	562.77
PBE+U	2.09	530.88	581.93
HSE	3.54	517.68	585.69
VASP-PBE	1.08 [39]	468.80 [40]	576.20 [40]
VASP-PBE+U	2.22 [39]	–	–

which are basically consistent with EPW. In addition, DFT +U and HSE modifications can be performed in our program, which enables relevant EPC studies in systems with strong correlated interactions. Moreover, we systematically compared the changes of EPC matrix of $LiCoO_2$ system under different functionals. We found that different functionals will lead to different results of EPC matrix for both electronic structure part and phonon structure part. Specifically, the electronic structure affects the relative values of the EPC matrix of the same phonon branch, while the phonon structure directly determines the relative values of the EPC matrix of different phonon branches. Analyzing the influence of electronic structure part and phonon structure part respectively can help us better understand the differences of the calculation results of EPC matrix under different functionals. Besides, it also demonstrates that the calculation of EPC matrix should choose more accurate functionals whether in electronic structure part or phonon structure part. We also found that PBE+U and HSE06 have basically the same results for calculating the EPC matrix. In this work, we select the experimental band gap values as the reference index of whether the electronic structure part is accurate, and select the experimental Raman peak positions as the reference index of whether the phonon structure part is accurate.

However, EPC is a broad research field, and the development of EPC matrix is just the beginning in this field. Some critical issues of EPC studies, such as fine-mesh interpolation, spin-orbital coupling effect, or density functional perturbation theory, might be implemented in future development. Based on this study, we will further expand and improve the code development of corresponding modules from the aspects of "theory-code-application" in future studies of electron phonon coupling.

This work was supported by the starting fund of Peking University Shenzhen Graduate School, Fujian Science & Technology Innovation Laboratory for Energy Devices of China (Grant No. 1C-LAB), the Chemistry and Chemical Engineering Guangdong Laboratory (Grant No. 1922018), the Soft Science Research Project of Guangdong Province (Grant No. 2017B030301013), and the Major Science and Technology Infrastructure Project of Material Genome Big-Science Facilities Platform supported by Municipal Development and Reform Commission of Shenzhen. The authors would like to thank Dr. Samuel Poncé from École Polytechnique Fédérale de Lausanne (EPFL) and Dr. Hyungjun Lee from University of Texas at Austin for their kindly help with some details about understanding EPW code.

Supporting Information

The supporting information is available online at tech.scichina.com and link.springer.com. The supporting materials are published as submitted, without typesetting or editing. The responsibility for scientific accuracy and content remains entirely with the authors.

1 Baroni S, de Gironcoli S, dal Corso A, et al. Phonons and related crystal properties from density-functional perturbation theory. Rev Mod Phys, 2001, 73: 515–562
2 Li J F, Pan Y, Wu C F, et al. Processing of advanced thermoelectric materials. Sci China Tech Sci, 2017, 60: 1347–1364
3 Zhang X, Qiao X F, Shi W, et al. Phonon and Raman scattering of two-dimensional transition metal dichalcogenides from monolayer, multilayer to bulk material. Chem Soc Rev, 2015, 44: 2757–2785
4 Giustino F. Electron-phonon interactions from first principles. Rev Mod Phys, 2017, 89: 015003
5 Xi J, Nakamura Y, Zhao T, et al. Theoretical studies on the deformation potential, electron-phonon coupling, and carrier transports of layered systems. Acta Physico-Chim Sin, 2018, 34: 961–976
6 Lazzeri M, Piscanec S, Mauri F, et al. Electron transport and hot phonons in carbon nanotubes. Phys Rev Lett, 2005, 95: 236802
7 Bloch F. Über die Quantenmechanik der Elektronen in Kristallgittern. Z Physik, 1929, 52: 555–600
8 Bardeen J, Shockley W. Deformation potentials and mobilities in nonpolar crystals. Phys Rev, 1950, 80: 72–80
9 Giustino F, Cohen M L, Louie S G. Electron-phonon interaction using Wannier functions. Phys Rev B, 2007, 76: 165108
10 Poncé S, Margine E R, Verdi C, et al. EPW: Electron-phonon coupling, transport and superconducting properties using maximally localized Wannier functions. Comput Phys Commun, 2016, 209: 116–133
11 Giannozzi P, Baroni S, Bonini N, et al. Quantum Espresso: A modular and open-source software project for quantum simulations of materials. J Phys-Condens Matter, 2009, 21: 395502
12 Zhou J J, Park J, Lu I T, et al. Perturbo: A software package for ab initio electron-phonon interactions, charge transport and ultrafast dynamics. Comput Phys Commun, 2021, 264: 107970
13 Zhou J J, Park J, Timrov I, et al. *Ab initio* electron-phonon interactions in correlated electron systems. Phys Rev Lett, 2021, 127: 126404
14 Zhou J J, Hellman O, Bernardi M. Electron-phonon scattering in the presence of soft modes and electron mobility in $SrTiO_3$ perovskite from first principles. Phys Rev Lett, 2018, 121: 226603
15 Miglio A, Brousseau-Couture V, Godbout E, et al. Predominance of non-adiabatic effects in zero-point renormalization of the electronic

band gap. npj Comput Mater, 2020, 6: 167
16 Brunin G, Miranda H P C, Giantomassi M, et al. Electron-phonon beyond fröhlich: Dynamical quadrupoles in polar and covalent solids. Phys Rev Lett, 2020, 125: 136601
17 Jia W, Cao Z, Wang L, et al. The analysis of a plane wave pseudo-potential density functional theory code on a GPU machine. Comput Phys Commun, 2013, 184: 9–18
18 Jia W, Fu J, Cao Z, et al. Fast plane wave density functional theory molecular dynamics calculations on multi-GPU machines. J Comput Phys, 2013, 251: 102–115
19 Li Z. Solid Theory (in Chinese). 2nd ed. Beijing: Higher Education Press, 2017. 18–60
20 Togo A, Tanaka I. First principles phonon calculations in materials science. Scripta Mater, 2015, 108: 1–5
21 Wannier G H. The structure of electronic excitation levels in insulating crystals. Phys Rev, 1937, 52: 191–197
22 Marzari N, Mostofi A A, Yates J R, et al. Maximally localized Wannier functions: theory and applications. Rev Mod Phys, 2012, 84: 1419–1475
23 Marzari N, Vanderbilt D. Maximally localized generalized Wannier functions for composite energy bands. Phys Rev B, 1997, 56: 12847–12865
24 Souza I, Marzari N, Vanderbilt D. Maximally localized Wannier functions for entangled energy bands. Phys Rev B, 2001, 65: 035109
25 Jain A, Hautier G, Ong S P, et al. Formation enthalpies by mixing GGA and GGA+U calculations. Phys Rev B, 2011, 84: 045115
26 Heyd J, Scuseria G E, Ernzerhof M. Hybrid functionals based on a screened coulomb potential. J Chem Phys, 2003, 118: 8207–8215
27 Mostofi A A, Yates J R, Pizzi G, et al. An updated version of Wannier90: A tool for obtaining maximally-localised Wannier functions. Comput Phys Commun, 2014, 185: 2309–2310
28 Jie J S, Weng M Y, Li S N, et al. A new MaterialGo database and its comparison with other high-throughput electronic structure databases for their predicted energy band gaps. Sci China Tech Sci, 2019, 62: 1423–1430
29 Vurgaftman I, Meyer J R, Ram-Mohan L R. Band parameters for III–V compound semiconductors and their alloys. J Appl Phys, 2001, 89: 5815–5875
30 Huang Z, Geyer N, Werner P, et al. Metal-assisted chemical etching of silicon: A review. Adv Mater, 2011, 23: 285–308
31 Yang Y, Yang J L, Pan F, et al. From intercalation to alloying chemistry: Structural design of silicon anodes for the next generation of lithium-ion batteries (in Chinese). Chin J Struct Chem, 2020, 39: 16–19
32 Poncé S, Antonius G, Boulanger P, et al. Verification of first-principles codes: Comparison of total energies, phonon frequencies, electron-phonon coupling and zero-point motion correction to the gap between ABINIT and QE/YAMBO. Comput Mater Sci, 2014, 83: 341–348
33 Goodenough J B, Kim Y. Challenges for rechargeable Li batteries. Chem Mater, 2009, 22: 587–603
34 Ye Y, Hu Z, Liu J, et al. Research progress of theoretical studies on polarons in cathode materials of lithium-ion batteries. Acta Phys Chim Sin, 2021, 37: 2011003
35 Liu T C, Pan F, Amine K. Prospect and reality of concentration gradient cathode of lithium-ion batteries (in Chinese). Chin J Struct Chem, 2020, 39: 11–15
36 Zhang M J, Chen Y S, Pan F, et al. Understanding structural evolution in the synthesis of advanced energy materials (in Chinese). Chin J Struct Chem, 2020, 39: 26–30
37 van Elp J, Wieland J L, Eskes H, et al. Electronic structure of CoO, Li-doped CoO, and $LiCoO_2$. Phys Rev B, 1991, 44: 6090–6103
38 Inaba M, Iriyama Y, Ogumi Z, et al. Raman study of layered rock-salt $LiCoO_2$ and its electrochemical lithium deintercalation. J Raman Spectrosc, 1997, 28: 613–617
39 Chakraborty A, Dixit M, Aurbach D, et al. Predicting accurate cathode properties of layered oxide materials using the SCAN meta-GGA density functional. npj Comput Mater, 2018, 4: 60
40 Du T, Xu B, Wu M, et al. Insight into the vibrational and thermodynamic properties of layered lithium transition-metal oxides $LiMO_2$ (M = Co, Ni, Mn): A first-principles study. J Phys Chem C, 2016, 120: 5876–5882